The reflection of pressure waves of finite amplitude from an open end of a duct

By GEORGE RUDINGER
Cornell Aeronautical Laboratory, Buffalo, New York

(*Received* 21 *May* 1957)

SUMMARY

When plane pressure waves in a duct reach an open end, they establish a complicated three-dimensional wave pattern in the vicinity of the exit which tends to readjust the exit pressure to its steady-flow level. This adjustment process is continually modified by further incident waves, so that the effective instantaneous boundary conditions which determine the reflected wave depend on the flow history. In the analysis of a nonsteady-flow problem by means of a wave diagram, it has been customary to assume that the steady-flow boundary conditions are instantaneously established. While this simplifying assumption appears reasonable, the resulting errors have been undetermined. It is the purpose of the present investigation to obtain improved boundary conditions. The results of a previous study of the reflection of shock waves from an open end have now been extended to other waves of finite amplitude. The reflected waves computed by means of the new procedure are in good agreement with experimental data observed in a shock tube for a variety of flow conditions. The pressure variations in a reflected wave lag behind those derived in the conventional manner by the time in which a sound wave travels about one or two duct diameters. Such lags are small, but may occasionally become significant. As a consequence of the lag, certain discontinuities of the incident wave do not reappear in the reflected wave. This improved understanding of the reflection process has made it possible to clarify some previously unexplained experimental observations.

1. INTRODUCTION

The reflection of pressure waves of finite amplitude from an open end of a duct must frequently be determined when quasi-one-dimensional nonsteady flows are being analysed by the method of characteristics. Such reflections are customarily computed under the assumption that the boundary conditions in nonsteady flow are the same as in steady flow (e.g. Shapiro 1954, p. 960; Rudinger 1955 a, p. 59). This assumption leads to convenient computing procedures, but represents only an approximation to the actual phenomena. The incident waves change the steady-flow exit pressure which, through the mechanism of a complicated three-dimensional wave pattern, can then re-establish itself only gradually at

a rate that depends on the time for waves to travel across the end section of the duct. Since this adjustment process is continually modified by the incident waves, the instantaneous boundary conditions depend on the history of the flow. Application of the steady-flow boundary conditions implies that the adjustment is instantaneous, so that the deviations of the exit pressure from its steady-flow level are neglected. The present investigation was undertaken to obtain improved boundary conditions which may be used instead of the conventional procedure or, at least, may permit an evaluation of the lag in the establishment of the steady-flow boundary conditions. Since wave-diagram procedures are based on the model of a one-dimensional flow, it is only necessary to find 'effective' boundary conditions. Details of the highly complicated three-dimensional flow phenomena in the immediate vicinity of the end section of the duct are not needed.

The work started with an analysis of the reflection of shock waves from an open end (Rudinger 1955 b), based on acoustic theory, and the results were in good agreement with experimental observations in spite of the finite amplitude of the waves considered. Therefore, it seemed promising to extend the analysis to arbitrary incident waves. The 'effective' pressure variations that occur in the end section of the duct during the adjustment process following the arrival of an incident shock wave may be considered as the 'response to a step function', from which the response to an arbitrary wave can be computed by means of Duhamel's integral. It is implied in this analysis that the steady-flow boundary conditions are represented by a constant pressure at the duct exit equal to that of the surrounding gas, but this boundary condition applies only to subsonic outflow from the duct. (The restriction to subsonic flow must be made because no reflected wave can propagate into the duct if the outflow velocity is sonic or supersonic.) If the direction of the velocity is reversed, and the gas flows from the surrounding gas into the duct, the pressure at the end is not constant, but becomes a function of the flow velocity, even in steady flow. The formation of a vena contracta, caused by flow separation at the inlet edge of the duct, further complicates the situation. The computing procedure derived from the results of the acoustic theory with the aid of Duhamel's integral strictly applies, therefore, only to outflow; but certain empirical modifications make it possible to deal also with inflow.

An experimental check on the results is obtained by measuring the pressure variations of the incident and reflected waves at some distance from the end of the duct where the flow can be considered as one-dimensional. From the data for the incident wave alone, the reflected wave can be computed on the basis of the new and the conventional procedures, and the results compared with the experimental observations.

2. Derivation of the computing procedure for subsonic outflow

In the previous study of the reflection of a shock wave from an open end (Rudinger 1955 b), the incident wave was expressed in terms of its

frequency spectrum by the Fourier integral of a step function. The Fourier integral of the reflected wave was then obtained from the known frequency dependence of the acoustic impedance of an open end. Numerical evaluation of this integral yielded the effective variations of the exit pressure, and the results were in good agreement with experimental observations. For weak shock waves, there are noticeable differences between the observed reflected wave and that computed by means of the conventional procedure. These differences become insignificant for stronger shock waves (i.e. with pressure ratios larger than about two in air). This is a fortunate finding, because the use of acoustic theory implies isentropic changes of state and applies, therefore, only to weak shock waves.

The deviations of the instantaneous pressure at the end of the duct $p_e(\tau)$ from the steady-flow value p_0 were expressed in terms of a dimensionless time

$$\tau = a_0 t/D, \tag{1}$$

where t is time measured from the instant of arrival of the shock wave at the exit, and a_0 is the initial speed of sound; the duct diameter D is the

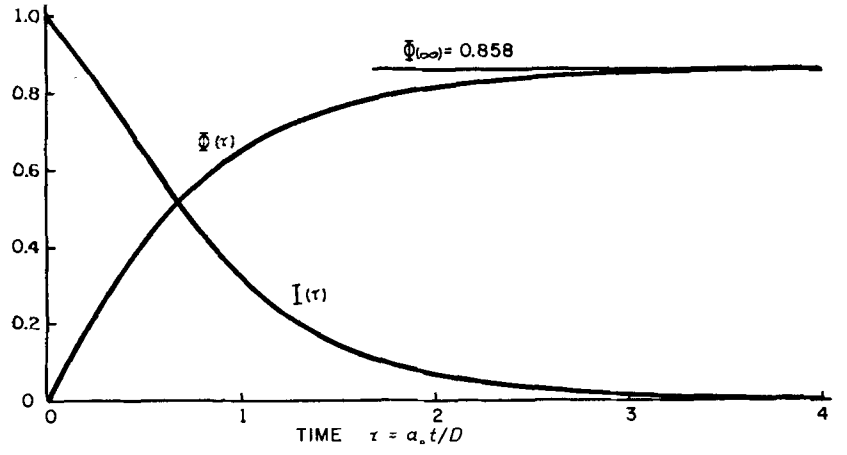

Figure 1. Plot of the functions $I(\tau)$ and $\Phi(\tau)$.

significant dimension that controls the rate at which the steady-flow boundary conditions are approached (see § 3 for further remarks on this). The result was obtained in the form

$$p_e(\tau) - p_0 = (p_i - p_0) I(\tau), \tag{2}$$

where $p_i - p_0$ is the pressure rise across the incident shock wave, and the time dependence $I(\tau)$ is shown in figure 1 (see also table 1). Equation (2) represents the instantaneous boundary conditions which can be applied in a wave diagram.

One may consider the function $I(\tau)$ as the indicial admittance of the system, that is, the response of the exit pressure to an incident wave in the form of a unit-pressure step. The response to an arbitrary incident wave,

described at the exit by $p(\tau)-p_0 = F(\tau)$, can then be derived by means of Duhamel's integral which may be expressed in the form (see, for instance, Kármán & Biot 1940, p. 403)

$$p_e(\tau)-p_0 = F(\tau_0)I(\tau-\tau_0)+\int_{\tau_0}^{\tau}\frac{dF(\theta)}{d\theta}I(\tau-\theta)\,d\theta, \tag{3}$$

where τ_0 is the instant at which the incident wave begins to arrive at the end of the duct, and θ denotes the integration variable. The wave diagram is started from an initial state of rest or steady flow; thus, the condition $F(\tau) = 0$ for $\tau \leqslant \tau_0$ eliminates the first term on the right side of equation (3).

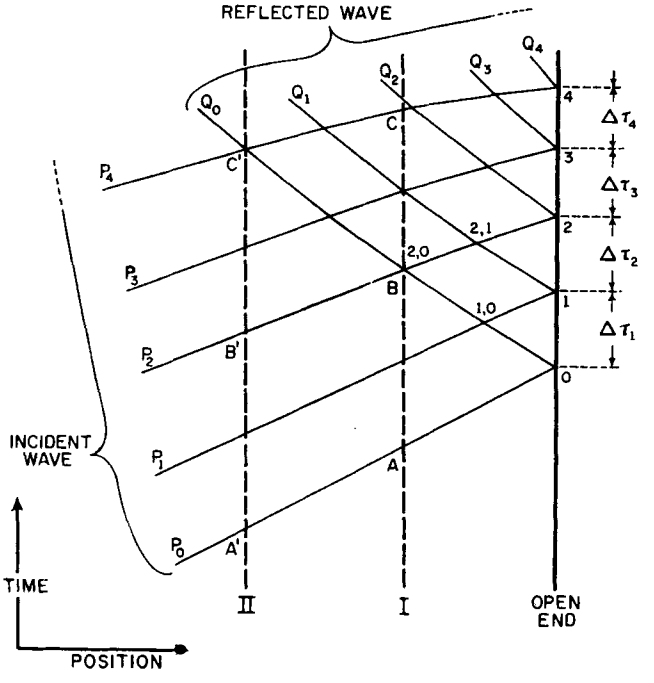

Figure 2. Wave reflections from an open end. I and II indicate the location of pressure transducers.

For $\tau > \tau_0$, the function $F(\tau)$ cannot, in general, be prescribed in advance, but becomes available only as the construction of the wave diagram proceeds. Figure 2 shows a sketch of the wave diagram which includes several characteristics of the incident wave (P_0, P_1, P_2...) and their reflections from the open end (Q_0, Q_1, Q_2...), which propagate with the velocities u_n+a_n and u_n-a_n respectively ($n = 0, 1, 2...$). The Riemann variables P_n and Q_n, defined by

$$P_n = 2a_n/(\gamma-1)+u_n, \tag{4a}$$

$$Q_n = 2a_n/(\gamma-1)-u_n, \tag{4b}$$

where γ has its usual meaning, remain constant along their respective characteristics if the flow is isentropic and the duct has a constant cross

section. (These assumptions do not restrict the present analysis, which is required to find only the wave that reaches the duct exit regardless of the manner in which the wave is generated. See § 3, where nonisentropic flow into the duct is considered.)

Regions between any two consecutive characteristics of the incident wave may be considered as small wave elements for which the derivative in the integrand of equation (3) can be replaced by the finite-difference ratio $\Delta F/\Delta\tau$. The flow conditions remain constant along a characteristic of the incident wave only until the latter interacts with the reflected wave. In the interaction region, the strength of a wave element must be measured along a crossing characteristic (see Rudinger 1955 a, pp. 31 & 32). The strength remains constant if expressed as a change of the speed of sound, but not if expressed as a change of pressure. Instead of calculating the pressure changes in the incident wave as modified by the reflected wave, it is therefore preferable to derive the boundary conditions directly in terms of the speed of sound, so that $F(\tau)$ must describe the incident wave in terms of this variable. The strength of an element of the incident wave Δa_n follows, from the property of characteristics (equations (4) with Q = const.), as

$$\Delta a_n = \tfrac{1}{4}(\gamma-1)(P_n - P_{n-1}). \tag{5}$$

This definition, apparently, neglects the last piece of the characteristics before they reach the exit. In figure 2, for example,

$$\Delta a_2 = a_{2,0} - a_{1,0} = a_{2,1} - a_1,$$

and the change of a between points 2, 1 and 2 is not considered. Actually, the incident wave element should be taken as $a_2' - a_1$, where the prime indicates the flow conditions that would be established if the duct did not terminate at this location after the arrival of the characteristic P_1. There would then be no reflected wave between 1 and 2, so that $Q_2' = Q_1 = Q_{2,1}$, and, therefore $a_2' = a_{2,1}$. This reasoning justifies the foregoing definition of Δa_n.

Interaction of the incident and reflected waves also modifies the times at which the characteristics of the former arrive at the open end. The actual arrival times, and therefore the values of $\Delta\tau_n$, can be taken directly from the wave diagram (see figure 2).

To derive a computing procedure in terms of the speed of sound rather than pressure requires that the indicial admittance be expressed in terms of this variable. Equation (2) defines $I(\tau)$ as a pressure ratio which is not exactly equal to the corresponding ratio of the sound speeds. Since the changes of state may be considered as isentropic, equation (2) may be rewritten in the form

$$I(\tau) = \frac{p_e(\tau)-p_0}{p_i-p_0} = \frac{(a_e/a_0)^{2\gamma/(\gamma-1)}-1}{(a_i/a_0)^{2\gamma/(\gamma-1)}-1} = \frac{a_e(\tau)-a_0}{a_i-a_0}\psi, \tag{6}$$

which defines a correction factor ψ that is always less then unity, because $a_i \leqslant a_e(\tau) \leqslant a_0$. Immediately after the arrival of the shock wave, when $a_e = a_i$, one obtains $\psi = 1$. The minimum value of ψ is reached when

a_e approaches a_0; but this error is insignificant because $I(\tau)$ then approaches zero. It seems reasonable, therefore, that any significant error would appear near the middle of the range where $a_e = \frac{1}{2}(a_i + a_0)$. For this value, a series expansion of ψ yields

$$\psi = 1 - \frac{1}{4}\left(\frac{\gamma+1}{\gamma-1}\right)\frac{a_i - a_0}{a_0} + \ldots . \tag{7}$$

For increments of $a_i - a_0$ not larger than about $0{\cdot}02a_0$, the value of ψ is then greater than 0·9 for any γ larger than 1·1. Such errors of the indicial admittance curve (see figure 1) could not be detected experimentally. Throughout the following, the relation

$$I(\tau) = \frac{a_e(\tau) - a_0}{a_i - a_0} \tag{8}$$

will therefore be used.

τ	$I(\tau)$	$\Phi(\tau)$	τ	$I(\tau)$	$\Phi(\tau)$
0	1·000	0	1·6	0·126	0·774
0·1	0·938	0·097	1·8	0·094	0·795
0·2	0·870	0·187	2·0	0·070	0·811
0·3	0·798	0·271	2·2	0·052	0·823
0·4	0·721	0·346	2·4	0·039	0·832
0·5	0·642	0·414	2·6	0·029	0·839
0·6	0·570	0·475	2·8	0·021	0·844
0·8	0·431	0·574	3·0	0·014	0·847
1·0	0·318	0·648	3·5	0·008	0·853
1·2	0·231	0·705	4·0	0·004	0·856
1·4	0·169	0·745	∞	0	0·858

Table 1. The functions $I(\tau)$ and $\Phi(\tau)$.

The boundary conditions at an open end can now be derived from equation (3) where, in view of the foregoing discussion, all pressures are replaced by the corresponding values of the speed of sound, and the derivative in the integrand is approximated by a step-wise constant function. The integral then breaks down into a series of terms each of which represents the contribution at the nth point from all preceding elements of the incident wave. One obtains

$$a_n = a_0 + \sum_{j=1}^{n} \frac{\Delta a_j}{\tau_j - \tau_{j-1}}[\Phi(\tau_n - \tau_{j-1}) - \Phi(\tau_n - \tau_j)], \tag{9}$$

where the function $\Phi(\tau)$ is defined by

$$\Phi(\tau) = \int_0^{\tau} I(\theta)\, d\theta. \tag{10}$$

The function $I(\tau)$ is known from the previous investigation, and the new function $\Phi(\tau)$ was derived from it by numerical integration. Values for both functions are listed in table 1. These numbers are uncertain within a few units in the last decimal place, but this accuracy is entirely adequate for wave diagram applications. A plot of $\Phi(\tau)$ is also included in figure 1.

Equation (9) represents the instantaneous boundary conditions. To illustrate the nature of the adjustment process at the duct exit, consider an incident compression wave $F(\tau)$ defined by

$$\left.\begin{aligned} \frac{dF(\tau)}{d\tau} &= (a_1-a_0)/(\tau_1-\tau_0) = \text{const.} && \text{for } \tau_0<\tau<\tau_1, \\ &= 0 && \text{for } \tau<\tau_0 \text{ and } \tau>\tau_1. \end{aligned}\right\} \tag{11}$$

It is not necessary, in this case, to divide the wave into small elements, since the values of $\Delta a_j/\Delta\tau_j$ would be the same for every element. Alternatively, one may consider the wave as one element of strength $\Delta a = a_1-a_0$ that is

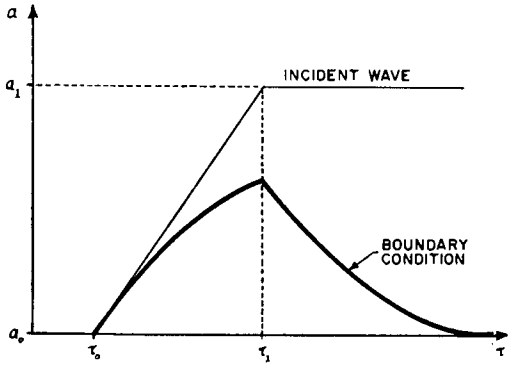

Figure 3. Variation of the flow conditions at the end section of the duct for an incident wave consisting of a single element.

arriving at the exit during the interval $\Delta\tau = \tau_1-\tau_0$. The boundary conditions then follow from (9), and are given by

$$\left.\begin{aligned} a &= a_0 && \text{for } \tau<\tau_0, \\ a &= a_0+\frac{a_1-a_0}{\tau_1-\tau_0}\Phi(\tau-\tau_0) && \text{for } \tau_0<\tau<\tau_1, \\ a &= a_0+\frac{a_1-a_0}{\tau_1-\tau_0}[\Phi(\tau-\tau_0)-\Phi(\tau-\tau_1)] && \text{for } \tau>\tau_1. \end{aligned}\right\} \tag{12}$$

These conditions are shown as the heavy line in figure 3. The values increase to a maximum given by

$$a_{\max} = a_0+\frac{a_1-a_0}{\tau_1-\tau_0}\Phi(\tau_1-\tau_0), \tag{13}$$

and then decay asymptotically. If τ_1 is large, the second term on the right side becomes small and $a_{\max}$ tends to a_0. This is exactly what one would expect, for, if the incident wave changes the flow conditions only slowly, the boundary conditions do not deviate significantly from their steady-flow values. If on the other hand, one considers the limit as $\tau_1-\tau_0$ tends to zero (incident shock wave), one obtains with the aid of equation (10)

$$\lim_{\tau\to 0}\Phi(\tau)/\tau \to I(0) = 1, \tag{14}$$

and, therefore, $a_{\max} = a_1$.

The procedure indicated by equation (9), applied to an incident wave for which $dF/d\tau$ is not constant, represents a superposition of the contributions from all wave elements that have reached the exit since the beginning of the wave. The difference of the Φ-functions in each term of the sum rapidly approaches zero when the smaller argument exceeds about three (see figure 2). In practice, one finds that only the most recent three or four wave elements contribute significant amounts to the sum. The increments after the end of the incident wave are all zero, but the calculations must be continued until all the contributions of the earlier elements have also decayed to zero.

This computing procedure is more complicated than the conventional one which is based on the simple boundary condition $a_n = a_0$, but the additional time required is not prohibitive. From a_n and P_n, one obtains u_n and Q_n by means of equations (4), so that the flow conditions and the reflected characteristic at the exit are completely determined.

3. Modification of the procedure for inflow

As discussed in § 1, the procedure derived in § 2 applies only to outflow from the duct, and some modifications are necessary before it can be applied to inflow. These modifications are of an empirical nature, and although they seem to be plausible, the results must be checked experimentally for a variety of flow conditions.

First, it is necessary to correct for the variation of the steady-flow boundary conditions with the velocity of inflow. The sum on the right side of equation (8) represents the deviation of the instantaneous from the steady-flow boundary conditions. For inflow, the steady-flow boundary conditions are not represented by the constant value a_0, but by $a_{n,\infty}$. The latter is related to the steady-flow velocity $u_{n,\infty}$ by the energy equation (see Rudinger 1955 a, pp. 63–65)

$$\frac{2}{\gamma-1}a_{n,\infty}^2+u_{n,\infty}^2=\frac{2}{\gamma-1}a_0^2, \tag{15}$$

where a_0, the speed of sound in the gas surrounding the duct, assumes the role of the stagnation condition. Since the Riemann variable P_n of the incident characteristic is known, equations (4 a) and (15) completely determine the flow that would be established if there were no lag in the adjustment to the steady-flow boundary conditions (as in the conventional procedure). Replacing a_0 by $a_{n,\infty}$ in equation (9) ensures, therefore, that the correct boundary conditions are obtained when a sufficiently long time has elapsed after the end of the incident wave.

The strength of every wave element Δa_j must also be modified to account for the change that the element causes in the steady-flow boundary conditions. For an incident expansion wave (to produce inflow) consisting of a single element specified by Δa and $\Delta\tau$, the largest deviation from the

steady-flow boundary condition occurs at the minimum value of a. The latter is given by the relation, analogous to equation (13),

$$a_{\min} = a_\infty + \frac{\Delta a_{\text{eff}}}{\Delta\tau}\Phi(\Delta\tau), \tag{16}$$

where Δa_{eff} represents the effective, modified strength of the wave element. This relation yields the correct value $a_{\min} = a_\infty$ for large $\Delta\tau$. It must also lead to $a_{\min} = a_0 + \Delta a$ ($\Delta a < 0$ for an expansion wave) in the limit as $\Delta\tau$ approaches zero. Because of equation (14), one obtains then $\Delta a_{\text{eff}} = \Delta a - (a_\infty - a_0)$, which shows that the strength of a wave element must be decreased by the associated change of the steady-flow boundary conditions. For a wave that is formed by a number of elements, the effective strength of any one must, therefore, be given by $\Delta a_j - (a_{j,\infty} - a_{j-1,\infty})$. The assumption implied in this analysis is that the functions $I(\tau)$ and $\Phi(\tau)$, which were derived for the adjustment process during outflow, can also be applied for inflow in spite of the different flow patterns in the two cases. With these modifications, equation (9) becomes

$$a_n = a_{n,\infty} + \sum_{j=1}^{n} \frac{\Delta a_j - (a_{j,\infty} - a_{j-1,\infty})}{\tau_j - \tau_{j-1}} [\Phi(\tau_n - \tau_{j-1}) - \Phi(\tau_n - \tau_j)], \tag{17}$$

which includes the outflow conditions as a special case, since it transforms into equation (9) for $a_{j,\infty} = a_0$.

So far only insentropic inflow has been considered, which is permissible only if the flow does not separate at the inlet edge of the duct. The losses associated with flow separation result in an entropy increase that must be taken into account. The characteristics of the incident wave must then pass through a region of variable entropy before they reach the end of the duct, and the values of P are no longer constant, but vary according to (e.g. Rudinger 1955a, pp. 18, and 39 & 40)

$$\frac{\delta_+ P}{\delta\tau} = a\frac{\delta_+ S}{\delta\tau}, \tag{18}$$

where $\delta_+/\delta\tau$ indicates the derivative in the characteristic direction $u + a$, and S is a dimensionless entropy (= entropy/$(\gamma - 1)\times$ specific heat at constant pressure) measured from the reference value $S_0 = 0$. Therefore it is necessary to find how the values of Δa_n are affected by the variations of P. The effect of entropy gradients can be derived with the aid of figure 4, which shows the incident characteristics at the exit points $n-1$ and n and the path of the gas 'particle' that separates the regions of zero and variable entropies; the 'particle' path entering the duct at the point $n-1$ is also indicated. Let $P_{n-1,0}$ and $P_{n,0}$ represent the Riemann variables of the two incident characteristics before they enter the region of variable entropy. In this region, the strength of the wave element is given by

$$\Delta a_{n,0} = a_{n,0} - a_{n-1,0} = \tfrac{1}{4}(\gamma - 1)(P_{n,0} - P_{n-1,0}). \tag{19}$$

The boundary conditions depend only upon waves that actually reach the end of the duct and, as stated before, the value of Δa_n should therefore express the change of the flow conditions that would be produced at the

location of the exit if the duct did not terminate there after arrival of the preceding wave element. Under these conditions, there would be no entropy change between k and n (see figure 4), so that

$$P'_n = P_k, \quad \text{and } Q'_n = Q_{n-1}. \tag{20}$$

Equations (4) yield

$$a'_n = \tfrac{1}{4}(\gamma-1)(P'_n+Q'_n), \quad \text{and } a_{n-1} = \tfrac{1}{4}(\gamma-1)(P_{n-1}+Q_{n-1}),$$

and, together with (20), lead to

$$\Delta a_n = a'_n - a_{n-1} = \tfrac{1}{4}(\gamma-1)(P_k - P_{n-1}). \tag{21}$$

Equation (18) can be integrated since a on the right side can be considered as a constant. This is always permissible in the cases considered here, because changes of a are small and aS is a sufficiently small quantity, so that

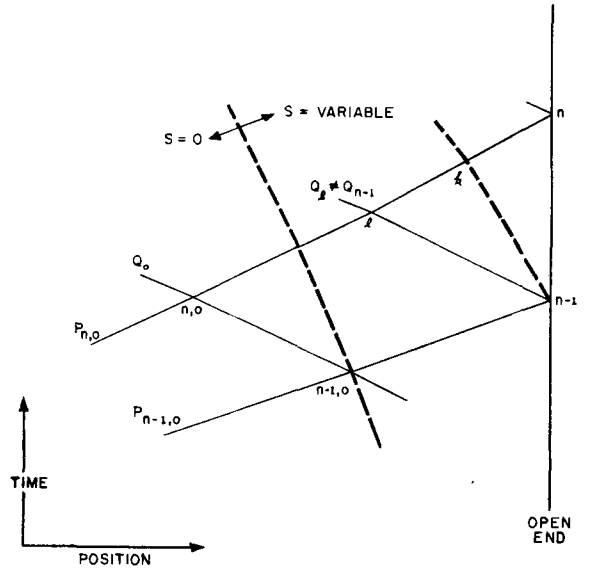

Figure 4. Reflection of a wave element that first traverses a region of variable entropy. The dashed lines indicate the path of gas ' particles ' along which the entropy remains constant.

the errors resulting from the foregoing simplification are negligible. The integration yields for the nth characteristic

$$P_n = P_{n,0} + a_{n,0}(S_n - S_{n,0}). \tag{22}$$

If this equation, applied to points k and $n-1$, is substituted into (21) and combined with (5) and (19), one obtains

$$\Delta a_n = \Delta a_{n,0}\{1 + \tfrac{1}{4}(\gamma-1)S_{n-1}\}, \tag{23}$$

where use has also been made of the condition $S_k = S_{n-1}$ (i.e. k and $n-1$ lie on the same 'particle' path). The intermediate wave-diagram point l is determined by P_l from equation (22), and Q_l from the analogous relation $Q_l = Q_{n-1} + a_{n-1}(S_l - S_{n-1})$, where S_l must be found by interpolation.

Equation (23) provides the desired correction for the strength of a wave element owing to its passage through the region of variable entropy, but the correction factor deviates from unity only by an insignificant amount. For sonic flow velocity into a sharp-edged duct inlet (Borda mouthpiece), the error would be less than 3% for $\gamma = 5/3$. In all actual cases, it would be even smaller, because the inflow velocity must be less than sonic for a characteristic to be able to reach the end of the duct. It can therefore be concluded that the strength of the incident wave elements may be determined from equation (19).

The values of $a_{n,\infty}$ in equation (17) can be obtained in the conventional manner from equations (4a) and (15), but P_n must first be computed from P_l or $P_{n,0}$ by means of equation (22). This step requires the yet unknown value of S_n. Some suitable assumptions must be made to determine this quantity. The inflowing gas forms a stationary vortex inside the duct, followed by a mixing region, after which the flow again fills the entire cross section (figure 5). In steady flow into a given inlet configuration, the entropy rise is a function of the flow velocity (or its speed of sound, since these two variables are related through equation (15)); in nonsteady flow, the changes of entropy lag behind those of velocity, because the former are a consequence of a mixing process which requires a certain time.

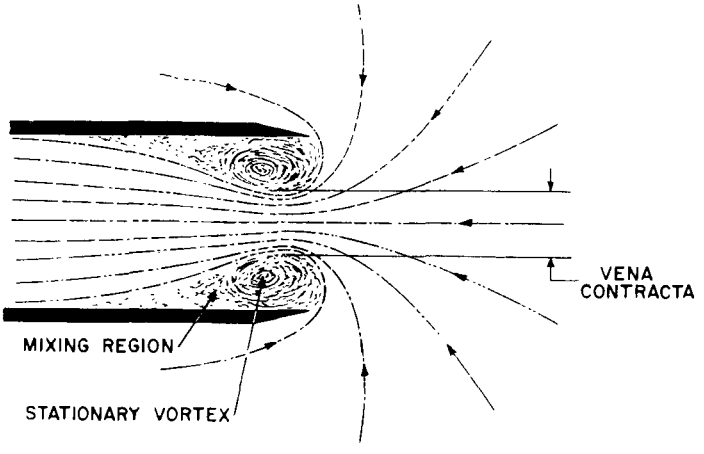

Figure 5. Flow into a duct with separation at the inlet edge.

The following simple assumptions have led to satisfactory agreement of the results with experimental observations. The vortex and subsequent mixing region are concentrated in the inlet section of the duct, and the entropy is given by

$$S_n = S_{n,\infty}. \tag{24}$$

To illustrate the last assumption, consider an incident expansion wave consisting of a single element. The speed of sound at the inlet drops from its initial value a_0 to some minimum, a_1, after which it gradually rises to $a_{1,\infty}$. The entropy, at the same time, rises from zero to S_1, which,

because of the lag, does not reach the level that would correspond to a_1 in steady flow; ultimately, the entropy becomes $S_{1,\infty}$. According to equation (24), the assumption is now made that $S_1 = S_{1,\infty}$.

These calculations require the steady-flow relation between entropy rise and flow velocity. Such a relation is readily computed for a sharp-edged inlet (Rudinger 1955 a, pp. 71–73), for which it takes the form

$$S_{n,\infty} = \frac{1}{\gamma} \log \left[\frac{1 + \{(a_0/a_{n,\infty})^2 - 1\} 2\gamma/(\gamma - 1)}{(a_0/a_{n,\infty})^{2\gamma/(\gamma-1)}} \right]. \tag{25}$$

In general, the entropy rise depends on the configuration of the duct, and must be given in any particular case by a relation or plot equivalent to equation (25). Since $a_{n,\infty}$ in this relation must be determined from P_n, which in turn depends on $S_{n,\infty}$, a certain amount of iteration may be required for this part of the calculations.

A further consequence of flow separation at the inlet is the formation of a vena contracta (see figure 5). The diameter of the stream tube that enters the duct, and in which the flow conditions must adjust themselves to the varying boundary conditions, is therefore smaller than the duct diameter. Accordingly, the significant length that is used in equation (1) to make the time variable nondimensional is assumed to be the diameter of the vena contracta D_c rather than the duct diameter D. The ratio of the cross-sectional area of the vena contracta to the duct area can be computed for a sharp-edged inlet as a function of the flow velocity (see, for instance, Busemann 1931, p. 377), and varies between 0·5 for low velocities (incompressible flow) and about 0·64 for sonic inflow. Accordingly, D_c/D varies between about 0·7 and 0·8. Variations of D_c/D for other inlet configuations might be determined by the method of Jobson (1955), but a constant average value $D_c/D = 0{\cdot}75$ was found to be satisfactory not only for a sharp-edged inlet, but also for a flanged inlet with a rounded edge (see § 4).

The inflow procedures may now be summarized as follows for point n of the wave diagram.

(1) Make an estimate for $S_n = S_{n,\infty}$, and compute P_n from equation (22). The required value of $a_{n,0}$ or a_l is already known from preceding wave diagram calculations.

(2) Determine $a_{n,\infty}$ from equations (4 a) and (15).

(3) Find $S_{n,\infty}$ from $a_{n,\infty}$ and the prescribed steady-flow relation between entropy and the speed of sound (equation (25) for a sharp-edged inlet or its equivalent for other configurations). If $S_{n,\infty}$ does not agree with the original estimate, repeat steps (1) to (3) with a new value until agreement is reached. These three steps also represent the conventional procedures which are based on $S_n = S_{n,\infty}$ and $a_n = a_{n,\infty}$.

(4) Determine Δa_n from equation (19).

(5) Compute a_n from equation (17), where the value $\tau = a_0 t/0{\cdot}75D$ is used. (This time variable must be used in equation (17), but it is not necessary to use D_c as the reference length for the entire wave diagram.) The required data for points $j < n$ are already known from preceding work.

(6) Compute u_n and Q_n from P_n and a_n with the aid of equations (4). With this step, the flow conditions at point n are completely determined, and the reflected characteristic can be plotted by means of the standard techniques.

4. Experimental check of the procedures

Experimental techniques

A shock tube constructed of a cold-drawn brass tube of 3·23 in. internal diameter was used for the experimental work. The length of the pressurized chamber was fixed at 12 ft., while the open duct was made up of several sections so that its length could be varied between 3 and 15·5 ft. Depending on the desired pressures, one or two sheets of photographic film or cellophane were used as diaphragms.

Two flush-mounted, condenser transducers (Rutishauser model HR3 with electronic indicator type ST–12) were available for pressure measurements. These had a range of 50 lb./in.^{2} and an adequate frequency response (the resonance frequency was of the order of 30 000 c/s). The pressure signals were displayed on a dual-beam oscilloscope (Dumont model 322A) and photographed on a drum camera (Southern Instruments model M–1020) at a film speed of 50 ft./sec. A second oscilloscope provided 0·1 millisecond timing marks that were recorded simultaneously with the pressure by means of an optical beam splitter arrangement. After each run, a calibration signal was recorded on the same film to check the sensitivity of the instrumentation. The calibration of the pressure recording system was linear over the range of the experiments. Two switches, built into the camera, served to blank the oscilloscope beams, except for one revolution of the drum, and to break the shock tube diaphragm at the right instant by means of a solenoid-operated needle.

The wave phenomena in the tube are indicated in figure 2. Comparison between theory and experiment is to be made at a point located 1 ft. from the open end (I). The incident wave reaches the transducer at A, and the reflected wave starts to arrive at B. After this time, the pressure record indicates the superposition of the two waves. A simple technique to determine the pressure distribution of the incident wave alone is to add an extension section to the shock tube which delays the arrival of the reflected wave sufficiently to record the incident wave over the range of interest in a separate experiment. The flow conditions associated with the incident wave are completely determined by the pressure record, since a follows from the condition of isentropic changes of state (wall friction effects are assumed to be small enough to be neglected)

$$\frac{a}{a_0} = \left(\frac{p}{p_0}\right)^{(\gamma-1)/2\gamma}, \tag{26}$$

and u follows from the property of the characteristics that $Q = Q_0$. Equation (4 b) yields, therefore,

$$u = 2(a-a_0)/(\gamma-1). \tag{27}$$

This method can only be used if the experiments are reproducible. Otherwise, the incident wave may be found with the aid of a second pressure transducer mounted 2 ft. from the open end. At this location (II), the incident wave can be recorded directly in the range between A' and C' (see figure 2) which is adequate for the present purpose.

In the regions A to B, and A' to B', both transducers record the incident wave alone. Equations (26) and (27) then serve as a check on their relative calibrations, since any pressure at location II appears at location I after a delay

$$t_{\mathrm{I}} - t_{\mathrm{II}} = L/(u+a), \tag{28}$$

where L is the distance between the pressure transducers. Equation (28) applies only to a simple wave for which the characteristics are straight lines. This property may also be utilized to detect condensation of water vapour in the region between the transducers, since one would no longer have a simple wave (see § 5).

Once the incident wave is determined by means of one of the two methods described, its reflection from the open end may be computed on the basis of the conventional and the new procedures. The interaction of these waves with the incident wave is then determined at location I, and the results are compared with the pressure record at this location.

Reflection of a compression wave

The compression wave was produced by placing a loosely fitting light piston into the shock tube a few inches downstream of the diaphragm; when the latter broke, the air pressure accelerated the piston thereby producing the compression wave. Proper selection of the weight of the piston, the pressure of the driving air, and the length of the duct, ensured that the compression wave had sufficient strength without steepening to a shock wave inside the duct, and that the wave reflected from the open end passed the points of pressure measurement before the piston arrived there. The piston was constructed of two $\frac{1}{8}$ in. discs of masonite separated by five wooden spacing rods of $3\frac{5}{16}$ in. length; its weight was about $\frac{1}{4}$ lb. The initial pressure difference across the shock tube diaphragm was 50 lb./in.^{2}, and the open end of the tube was 15·5 ft. from the diaphragm. A new piston had to be used for every run, and instead of relying on the reproducibility of the experiments, the incident wave was determined by means of the described technique based on two pressure transducers. The results obtained in this manner are presented in figure 6. Although the incident wave has just steepened sufficiently to form a weak leading shock wave, most of the pressure rise in the incident wave takes place gradually. The presence of a shock front requires that the term $\Delta a_{\mathrm{shock}} I(\tau - \tau_0)$ (from (8)) be added to the boundary conditions given by (9). The experimental results for the reflected wave are in good agreement with the data based on the new procedure, while the conventional technique indicates too rapid a pressure drop.

Reflection of an expansion wave

The shock-tube chamber was evacuated instead of pressurized in these experiments, and to obtain sufficiently steep expansion waves, the distance from the diaphragm to the open end was made rather short; it was 3·25 or 4·25 ft. depending on whether one or two pressure transducers were used. Initial pressure differences across the diaphragm were varied between -2 and -13 lb./in.^{2}

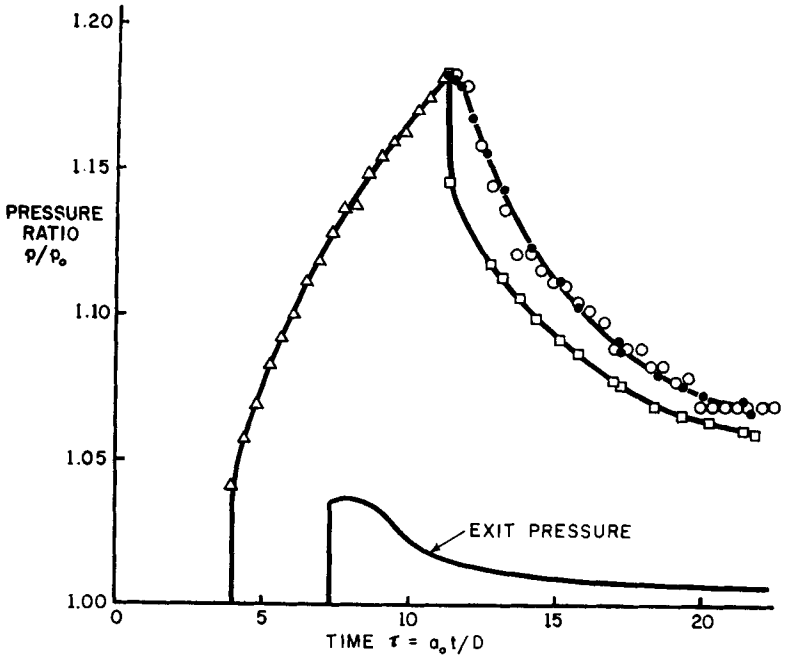

Figure 6. Reflection of a compression wave. Comparison of theory and experiment at 1 ft. from the open end of a duct of 3·23 in. diameter. The time is measured from the arrival of the incident wave at 2 ft. from the end. Experimental data : Δ incident wave; o interaction of incident and reflected waves. Computed data : • new boundary conditions, □ steady-flow boundary conditions. The computed ' effective ' exit pressure ratio is also plotted.

A sufficiently weak incident wave passes the pressure transducer completely before the reflected wave arrives so that both waves can be measured directly in one experiment with a single transducer. For stronger waves, the two waves interact at the location of the transducer and the incident wave must be found by other means. Since the pressure records were reproducible, it was possible to use the method of the tube extension described in the foregoing, although the alternative method based on two pressure transducers was also employed.

All experiments, with one exception, were carried out with a sharp-edged inlet (Borda mouthpiece) because the entropy rise is then readily determined. The results for this configuration and for initial diaphragm pressure differences of -2, -5, and -13 lb./in.^{2} are shown in figure 7 as curves *a*,

b and *c* respectively. It is seen that the customarily used steady-flow boundary conditions predict a pressure rise in the reflected wave that is faster than the one actually observed, while the new procedure leads to good agreement with the experimental data for the two weaker waves. For the strongest wave *c*, the agreement is still good at the beginning of the reflected wave, but the computed values gradually rise faster than the experimental ones (see § 5).

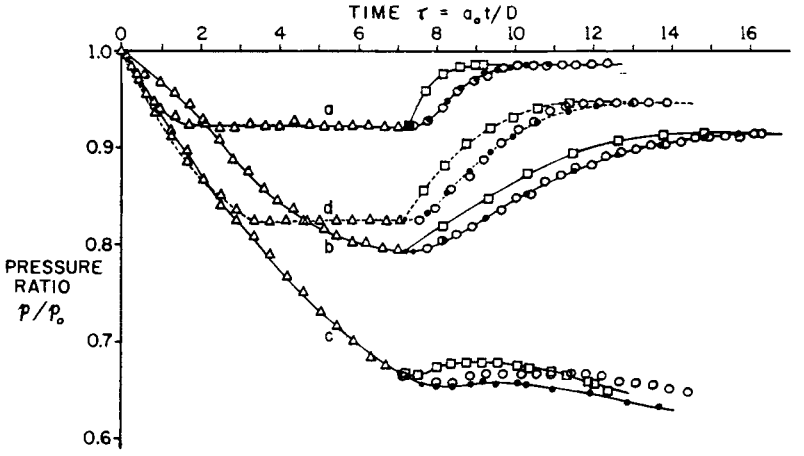

Figure 7. Reflection of expansion waves. Comparison of theory and experiment at 1 ft. from the open end of a duct of 3·23 in. diameter; *a*, *b*, *c* sharp-edged inlet for initial diaphragm pressures of −2, −5, and −13 lb./in.^{2} respectively; *d* flanged inlet with rounded edge; initial diaphragm pressure −5 lb./in.^{2} (See figure 6 for explanation of the symbols.)

One experiment was carried out with an inlet configuration consisting of a flanged duct with a rounded inlet edge, and an initial diaphragm pressure difference of −5 lb./in.^{2}. From the measured steady-flow pressures after the incident and reflected waves, respectively, the entropy rise for the final steady-flow velocity could be computed and was found to be 61% of that of a sharp-edged inlet for the same flow velocity. The entropy rise at the other flow velocities was then assumed to be given by the same fraction of the corresponding value for a sharp-edged inlet. The results for this experiment, plotted as curve *d* in figure 7, show the same good agreement between the computed values based on the new boundary conditions and the experimental data. (The incident waves for cases *b* and *d* are different in spite of the same initial pressure conditions, because the diaphragm materials were not the same in these experiments; photographic film was used for *b* and cellophane for *d*. These variations do not affect the results, since the evaluation of the experiments is always based on the individual incident wave.)

5. Discussion and conclusions

The previously derived boundary conditions for the reflection of shock waves from an open end have been extended to other waves. As long as

subsonic outflow from the duct is maintained no further assumptions are required. Since the analysis for shock waves led to good agreement with experimental observations, one should expect similar agreement for other waves for which the disturbance at the duct exit is less violent. This is indeed observed, as indicated by figure 6. As additional interesting information, the variations of the effective exit pressure were obtained from the wave diagram that had to be prepared for the evaluation of the experiment, and these are also plotted in figure 6. It is seen that this pressure, after an appreciable disturbance, tends to readjust itself to the steady-flow value p_0, but levels off slightly above p_0 where it remains almost constant as long as the incident wave 'tries' to raise the pressure.

The computing procedures had to be modified to make them applicable to inflow. Because of the empirical nature of the modifications, it was important to verify their consequences for a variety of flow conditions. The described modifications are the ones found to be most satisfactory, and the good agreements between calculated and experimental data to which they lead is demonstrated in figure 7. A disagreement was found only for the strongest waves (*c*), and then only for the later portion of the reflected wave when the observed pressures rise higher than those computed on the basis of the steady-flow boundary conditions. Since the difference between the two theoretical curves is caused by the lag in the establishment of the steady-flow boundary conditions, one must conclude that the discrepancy cannot be caused by an error in the evaluation of this lag. Any uncertainty about the incident wave that might have been caused by the effects of condensation of water vapour in the duct was also ruled out by the described technique of using two pressure transducers. The recorded pressures were found to be related to each other exactly in the manner required by equations (26) to (28) for a simple wave, which indicated the absence of condensation effects. This finding seems to leave wall friction effects as the only cause for the observed discrepancy between theory and experiment. In this case, the flow in the vena contracta has already become sonic, and the Mach number of the flow exceeds 0·5 further inside the duct. A crude analysis of the friction effects by a linearization method, similar to that of Trimpi & Cohen (1955), indicates that a friction coefficient several times that of its steady-flow value could indeed explain the discrepancy. This result appears reasonable in view of the uncertainty of the friction coefficient for nonsteady flow in the vicinity of a sharp-edged inlet.

It is apparent from figures 6 and 7 that the actual flow conditions lag behind those computed in the conventional manner by about the time in which a sound wave travels one or two duct diameters. The corresponding lag time for shock reflection is (see figure 1) the travel time for about three duct diameters.

An interesting consequence of the lag is the elimination of certain discontinuities of the incident wave from the reflected wave. Figures 6 and 7, for instance, show clearly that the derivative $\partial p/\partial \tau$ has a discontinuity at the head of the incident wave which reappears at the head of the reflected wave only when the conventional boundary conditions are used, while the

George Rudinger, The reflection of pressure waves of
finite amplitude from an open end of a duct, Plate I.

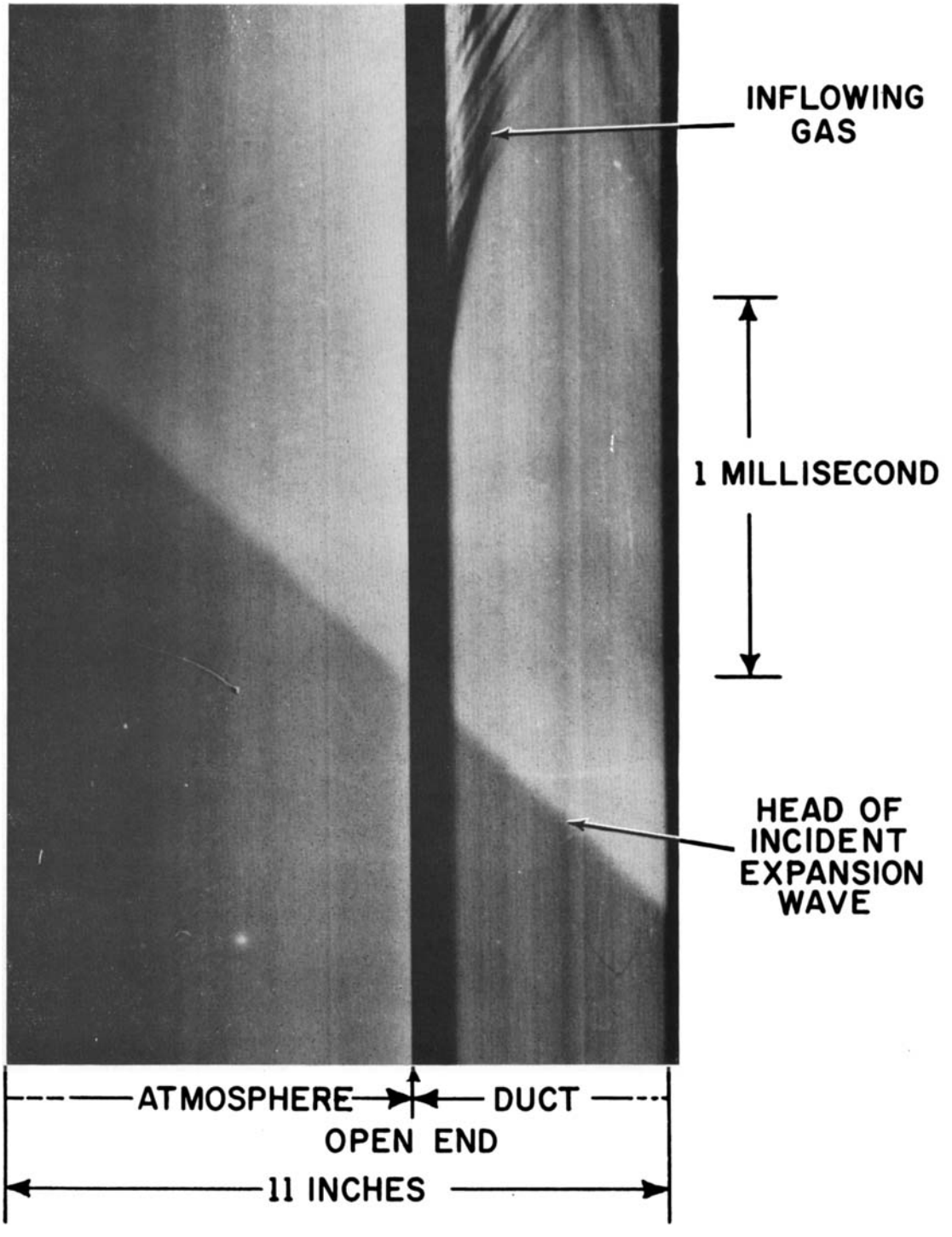

Figure 8. Schlieren streak record of the reflection of an expansion wave from an open end of a 3 × 3 in. shock tube. Note the apparent absence of a reflected wave. (Courtesy of Dr I. I. Glass, University of Toronto.)

new boundary conditions, in agreement with the experimental data, indicate a gradual change of the slope of the curves. A general proof for this observation can be obtained by differentiating equation (3) with respect to τ which yields

$$\frac{dp_e(\tau)}{d\tau} = \frac{dF(\tau)}{d\tau} I(0) + \int_{\tau_0}^{\tau} \frac{dF(\theta)}{d\theta} \frac{dI(\tau-\theta)}{d\tau} d\theta, \tag{29}$$

where $I(0) = 1$. The integral in this relation is a continuous function of τ if $F(\tau)$ is continuous, so that any discontinuities of $dp_e/d\tau$ are fully accounted for by those of the derivative of the incident wave alone. Consequently, no discontinuities appear in the reflected wave. The significance of this conclusion becomes evident if one considers that a schlieren photograph of a gas flow does not record gas densities but density gradients. The discontinuity of the gradient at the head of an expansion wave in a shock tube is therefore readily photographed, while the head of the wave reflected from an open end, having no such discontinuity, would appear on the record only faintly, if at all. This phenomenon was actually observed at the University of Toronto (Glass & Patterson 1955), where schlieren streak records of this reflection process were obtained. The relevant portion of such a record is reproduced in figure 8 (plate 1), and the originally puzzling observation of an apparently missing reflected wave is now quite understandable.

In conclusion, it may be stated that new boundary conditions for wave reflection from an open end have been derived which lead to a better agreement with experimental observations than the customarily used steady-flow boundary conditions. The new procedures take into account that the steady-flow boundary conditions are not instantaneously established, and that the adjustment process is continually modified by the incident waves. The actual flow conditions lag behind those computed in the conventional manner and, although the lag times are small, they may occasionally become significant. The new computing procedures are more complicated than the conventional ones, but the additional time required for their application is not prohibitive. On the other hand, one must also consider that the resulting refinement may not be warranted because of other errors introduced into a wave diagram by some simplifying assumptions, such as the neglect of wall friction at high flow velocities. It has also been shown that certain discontinuities of the incident wave are eliminated from the reflected wave. This improved understanding of the reflection phenomena made it possible to explain certain, previously puzzling, experimental observations.

This work was sponsored by Project Squid which is supported by the Office of Naval Research under Contract N6-ori-105, T.O. III. The author is greatly indebted to Mrs Angela Chang who prepared the many wave diagrams that were needed to test various modifications of the procedures for inflow and who also contributed suggestions for such modifications, and to Mr L. M. Somers who carried out the shock-tube experiments.

References

BUSEMANN, A. 1931 *Handbuch der Experimentalphysik*, Vol. IV, Part 1. Akad. Verlagsgesellschaft.

GLASS, I. I. & PATTERSON, G. N. 1955 A theoretical and experimental study of shock-tube flows, *J. Aero. Sci.* **22**, 73.

JOBSON, D. A. 1955 On the flow of a compressible fluid through orifices, *Proc. Inst. Mech. Engrs.* **37**, 767.

KÁRMÁN, TH. V. & BIOT, M. A. 1940 *Mathematical Methods in Engineering*. New York : McGraw-Hill.

RUDINGER, G. 1955 a *Wave Diagrams for Nonsteady Flow in Ducts*. Princeton : Van Nostrand.

RUDINGER, G. 1955 b On the reflection of shock waves from an open end of a duct, *J. Appl. Phys.* **26**, 981.

SHAPIRO, A. H. 1954 *The Dynamics and Thermodynamics of Compressible Fluid Flow*, Vol. II. New York : Ronald.

TRIMPI, R. L. & COHEN, N. B. 1955 A theory for predicting the flow of real gases in shock tubes with experimental verification, *Nat. Adv. Comm. Aero., Wash., Tech. Note* no. 3375.